NANO LETTERS

2003
Vol. 3, No. 8
1087−1090

Interparticle Coupling Effects on Plasmon Resonances of Nanogold Particles

K.-H. Su, Q.-H. Wei, and X. Zhang*

Mechanical & Aerospace Engineering Department, University of California at Los Angeles, Los Angeles, California 90095

J. J. Mock, D. R. Smith, and S. Schultz

Department of Physics, University of California at San Diego, La Jolla, California 92093

Received April 2, 2003; Revised Manuscript Received June 6, 2003

ABSTRACT

The collaborative oscillation of conductive electrons in metal nanoparticles results in a surface plasmon resonance that makes them useful for various applications including biolabeling. We investigate the coupling between pairs of elliptical metal particles by simulations and experiments. The results demonstrate that the resonant wavelength peak of two interacting particles is red-shifted from that of a single particle because of near-field coupling. It is also found that the shift decays approximately exponentially with increasing particle spacing and become negligible when the gap between the two particles exceeds about 2.5 times the particle short-axis length.

Noble metal nanoparticles, usually of Ag or Au, are well known for their strong interactions with visible light through the resonant excitations of the collective oscillations of the conduction electrons within the particles. As a result, local electromagnetic fields near the particle can be many orders of magnitude higher than the incident fields, and the incident light around the resonant-peak wavelength is scattered very strongly. This local-field enhancement and strong scattering have been proven to be very unique for biomolecular manipulation, labeling, and detection.[1,2]

The enhanced electric fields are confined within only a tiny region of the nanometer length scale near the surface of the particles and decay significantly thereafter. This localized field enhancement provides a field gradient that is much greater than that of any far-field optical tweezers; therefore, it may be possible to trap single molecules or other nanoparticles in regions near an elliptical metal nanoparticle or tip[3−5] or between two nanoparticles.[6] It has also been shown that the emission properties of fluorescent molecules under the influence of this enhanced field are changed dramatically. As an example, the radiative decay rates and quantum yields of weakly fluorescent species can increase significantly. Even multiphoton absorptions and fluorescence excitations have been shown to be possible.[7,8] The recent discovery of single-molecule sensitivity of Raman scattering enhanced by resonantly excited metal nanoparticles has caused a renewed interest in surface-enhanced Raman scattering (SERS) and its application to molecular detection.[9−11]

In typical SERS experiments, a collection of colloidal particles of various sizes are induced to aggregate, and those aggregates that happen to be resonantly excited by the illuminating laser are called “hot spots”. Therefore, from a practical point of view, it is very important to be able to fabricate optimally designed plasmon configurations of interacting nanoparticles.

The resonant frequency of a metal nanoparticle is known to be dependent on its size, shape, material properties, and surrounding medium.[12−14] When a cluster of metal nanoparticles are placed in close proximity to one another, such as in SERS experiments, the coupling between particles becomes very important.[11,15−17] In this paper, we focus our study on the effects of near-field interparticle coupling on the particle plasmon resonances, especially the shift of the plasmon resonant wavelength as a function of particle separation. As expected, the experimental and simulation results indicate that the resonant wavelength of two coupled particles in close proximity is significantly red-shifted from that of the individual particles. This shift decays approximately exponentially with increasing particle spacing. It is also found that the exponential decay of the peak shift with the particle gap is size-independent because the shift and gap are scaled respectively by the peak wavelength and

* Corresponding author. E-mail: xiang@seas.ucla.edu.

10.1021/nl034197f CCC: $25.00
Published on Web 06/21/2003

particle sizes. The scaled decay function is particle-shape-dependent in the sense that the decay length depends on particle shapes. We note that the shift drops to zero when the gap between the two particles reaches about 2.5 times the particle size.

The gold nanoparticles were prepared on quartz substrates by electron-beam lithography (EBL) and the standard lift-off process, which allows for the accurate placement of the particles on designed locations. To reduce charging effects during the EBL, 10-nm-thick indium tin oxide (ITO) films were sputtered on the quartz substrates. Polymathylmethaacrylate (PMMA) films (100 nm thick) were spin-coated on this ITO−quartz glass, which was used as a positive photoresist for e-beam lithography. The samples were examined by a scanning electron microscopy (Hitachi) to characterize the size and shape of these nanoparticles.

Evanescent light produced by a collimated light beam undergoing total internal reflection (TIR) is utilized to excite the particle plasmons. The excited collective electron oscillations within the particles then radiate electromagnetic waves of the same frequency into the far field, whereby the collection and spectral measurement take place. In our experiments, a collimated light beam delivered by a multimode optical fiber from a 75-W Xe white-light source is incident on a right-angle prism at an angle resulting in total internal reflection. The samples are situated on the top surface of the prism, and index-matching oil is used between the touching surfaces of the sample substrate and the prism, which ensures that all stray scattering light due to surface defects and dust particles is minimized, leading to very high dark-field contrast. The scattered light from the metal nanoparticles is collected by an optical microscope with a 50× long-working-distance objective and forms an image at the image plane. At this image plane, a small aperture is located to select individual particles or pairs of particles and serves to block the scattered light from the surrounding particles and substrate. The emerging light is then imaged onto the entrance slit of an SPEX 270M grating spectrometer system with a thermal electrically cooled charge-coupled device (CCD) detector (Princeton Instruments). The detailed experimental setup has been described in a previous paper.[12]

To demonstrate the control of the plasmon resonant wavelength of single particles, we first fabricated well-separated gold nanoparticles of various sizes. Usually, a thin, 5-nm Cr layer is deposited before the Au deposition to promote the adhesion between Au and the quartz substrates. The vertical thickness of the particles is kept at 30 nm in our study. As shown in Figure 1a, the particles are slightly elongated, and the ratio between the long and short axes is about 1.55. To study the coupling effects of two particles on their common plasmon resonance, we have also fabricated particle pairs with various interparticle spacing and sizes. We denote a line connecting two centers of coupled particles as the *x* axis. It was determined that the particle short axis is tilted about 7° from the *x* axis. The purpose of fabricating tilted elliptical particle pairs is to see the effect of the tilt angle on plasmon couplings. For measurements of both single particles and particle pairs, the polarization of the incident-

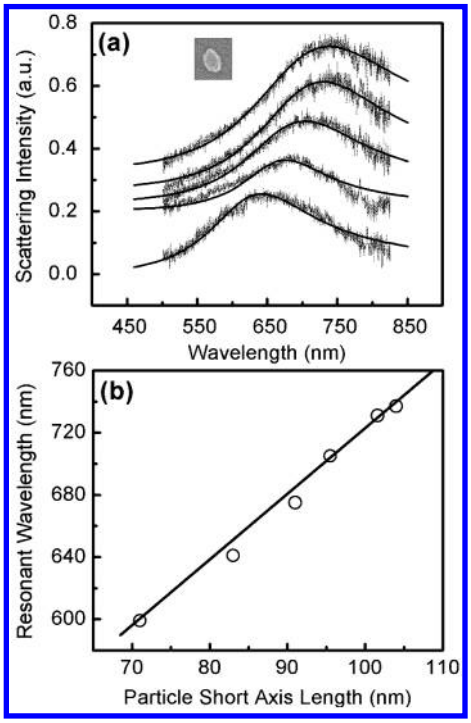

Figure 1. (a) Scattering spectra of elliptical Au particles with short-axis lengths of 84, 91, 96, 102, and 104 nm. The long/short axis aspect ratio is kept at about 1.55. (b) Measured plasmon resonant wavelength as a function of the particle short-axis length.

light electric field is selected parallel to the *x* axis. In the EBL process, the individual particles or particles pairs are well separated from each other; therefore, multiparticle interference effects or so-called long-range dipole interactions on the spectrum measurements are eliminated.

Figure 1a presents some typical measured scattering spectra of single nanoparticles with the short axis varying from 84 to 104 nm and with a long/short axis ratio about 1.55. Owing to the TIR dark-field illumination and the strong plasmon-resonance-associated scattering, individual nanoparticles can be easily identified and distinguished from dust. It is clear that the plasmon-resonant-peak wavelength is shifted significantly to larger values with increasing particle size. A plot of the peak resonant wavelength as a function of particle size indicates a good linear relationship (Figure 1b), in agreement with Mie scattering theory.

The effect of particle size on the peak resonant wavelength results from two different mechanisms depending on the particle size range. For small particles with diameters of less than 10 nm, known as the quasi-static regime, the effects of phase retardation and multiple modes can be neglected. Whereas Mie theory gives a constant resonant frequency independent of particle size if the bulk dielectric constant is used, the size effect in the quasi-static regime comes from the dependence of the permittivity on particle size because of quantum confinements. For larger particles with diameters greater than 10 nm, such as in our case, the quantum confinement effect or size dependence of dielectric coefficients becomes negligible, and the role of phase retardation effects comes into play. The peak red-shift observed in our experiments is a fully electrodynamic effect due to phase

retardation. With this linear relationship between resonance frequency and size, it is easy for a researcher to design the target illumination wavelength of hot spots in SERS applications.

As a result of the elliptical particle shape, there should be two resonant frequencies corresponding to the long and short axes. Obviously, the incident electrical field along the particle center−center axis should lead to a component along both the long and short axes of the particles. With a particle tilt angle of only 7°, the plasmon resonance peak corresponding to the long axis is not sufficiently excited because the projected electric-field component is too small. This was confirmed by computer simulations. We note that we did observe the two peaks for individual particles of 114 nm/72 nm size with a 16° angle between the electric field and the particle short axis.

To compare these results with theory and to design the particle parameters for required resonant wavelength, we performed computer simulations using the discrete dipole approximation (DDA). We thank Draine and Flatau for their code and for making it accessible.[18] A description of the DDA simulation code and its effective applications to particle plasmon resonance can be found in refs 17, 19, and 20. We use the dielectric constant of bulk Au as measured by Johnson and Christy.[21] As is known, the plasmon resonance is sensitive to the surrounding medium, and the ITO glass substrate has a strong effect on the plasmon resonant wavelength.[20] Instead of attempting a complete solution, Tamaru et al. have shown that the effect of the substrate can be taken into account to a first-order approximation by embedding the particles in a homogeneous medium with a refractive index equal to the average refractive index value of the substrate and surrounding medium (air in our case).[22] Given that the refractive index of ITO is about 2 and that air is 1, we used 1.5 as the refractive index of the surrounding medium. With substrate effects implemented in this way, the DDA simulations without any free parameters show good agreement with the single elliptical particle plasmon resonances, as exemplified by the curve in Figure 2a. Figure 2a shows the simulation results for the scattering spectra of two ellipsoid disks as a function of particle center−center spacing. The long and short axis lengths of the particles are 130 and 84 nm, respectively, and the disk thickness is 30 nm. The polarization of the incident light beam is parallel to the *x* axis, and the particle short axis makes a 7° angle with respect to the *x* axis. One can observe that the resonant peak has significantly red-shifted for short particle spacing, indicating strong plasmon coupling. When the particle center−center spacing is set larger than 258 nm, the resonance peak barely changes with further spacing increases, reaching the single-particle resonance. This single-particle plasmon resonance peak is in close agreement with the measured value (Figure 1). The peak width at half intensity (∼100 nm), however, is much narrower than that in our experiments (∼180 nm). This discrepancy is attributed to the thin layer of Cr that induces a damping loss, as is confirmed by the experimental observation that without a Cr adhesion layer the measured peak width is ∼100 nm. Figure 2b shows the resonant

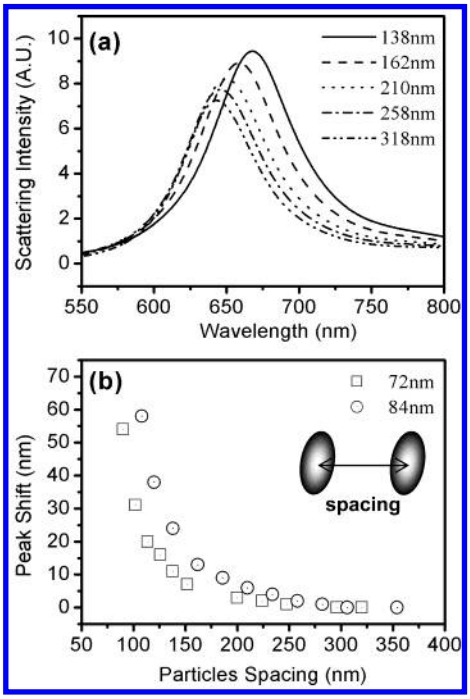

Figure 2. (a) Simulated scattering spectra of two coupled Au elliptical disks. The short axis is kept at 84 nm, and the long/short axis ratio, at 1.55. The center−center particle spacing is varied from 138 to 318 nm. (b) Resonant-peak wavelength as a function of particle center−center spacing for particles with short-axis lengths of 72 and 84 nm.

wavelength shift as a function of the center−center spacing between two particles for two different particle sizes. The peak shift decays rapidly with increasing particle spacing, reaching zero when the particle spacing exceeds certain distances, indicating the diminishing of the near-field plasmon coupling between these two elliptical particles. These reductions in peak shift and scattering intensity with particle spacing reflect the decaying of the field distribution between the particles, which plays a key role in particle plasmon applications such as SERS[9−11,23] and nano-optics.[24−26]

We have also simulated plasmon couplings of other particle sizes with the same aspect ratio. As in the experiments, the polarization is set parallel to the particle center−center axis. It is observed that the resonant peak shifts are significantly different for different particle sizes. Interestingly, when the peak shift is scaled by the peak wavelength and the gap is scaled by the particle short-axis length, all data points fall on a common curve (Figure 3). A least-squares fit shows that the decay of the peak shift can be approximated as an exponential function, with the shift dropping to zero as the particle gaps exceed about 2.5 times the particle short axis. It is worth noting that other functions such as a power law decay can be fitted with equal accuracy, although we take the exponential decay as a plausible fitting function based on the following considerations. First, it is known that when two identical resonators are coupled the resonance frequency will shift relative to that of the uncoupled single resonator, with the shift proportional to the coupling coefficient if the shift or the coupling coefficient is small. Therefore, the behavior of the resonance wavelength shift as a function of the particle gap reflects the behavior

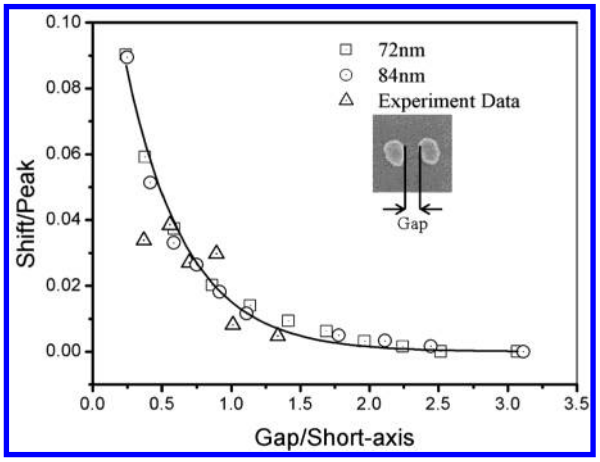

Figure 3. Comparison of computer-simulated (□, ○) and experimentally (△) measured resonant wavelength shifts as a function of the gap between two particles.

of near-field plasmon coupling. The resonant plasmons of two Au particles are coupled with each other by photons tunneling through the gap between them. As usual in many other cases of quantum and classical wave tunneling such as evanescent coupling in optical waveguides, the coupling coefficient can be approximated as an exponential function of the gap between them. This is also the reason that the particle edge−edge gap, instead of the particle center−center spacing, is used in Figure 3.

We fabricated particle pairs at various distances and sizes while retaining the same particle long/short axis ratio. The experimental results are shown in Figure 3. It can be seen that these data agree well with the simulation curve. We have also carried out additional computer simulations for the scaling of the resonance wavelength shift for different particle shapes. The results indicate that the scaling phenomenon is valid for different particle shapes and that all peak shifts can be approximated as exponential decays with the particle gap. The decay lengths, however, are dependent on particle geometric shapes. The scaling of the shift value as a function of the interparticle gap will not only be very useful for designing coupled particles for the desired excitation wavelengths for SERS applications but will also help provide a deeper understanding of plasmon coupling for near-field optics.

In conclusion, we have studied the plasmon coupling between two elliptical particles and have found that the plasmon resonant peaks are significantly shifted to higher wavelength as the interparticle spacing is reduced. The peak shift is found to be well described as an exponential function of the gap between the two particles and drops to negligible values when the gap is larger than about 2.5 times the short-axis length. This exponential decay is found to be size-independent when the peak shift and particle gap are scaled respectively by the resonant-peak wavelength and the short-axis length of the individual particles. The decay length, however, is found to be particle-shape-dependent. These results can be used as a guideline for designing and fabricating SERS-active substrates for ultrasensitive molecular detections.

Note Added in Proof. After submitting this paper, we learned from one anonymous referee that there is an interesting paper with related content.[27]

Acknowledgment. The work at UCLA was supported by an NSF CAREER award (DMI-01963951) and an ONR Young Investigator award (N00014-02-1-0224). The work at UCSD was supported by DOE DEFG03-01-ER45881. We thank Xiaoxiao Zhang, P. J Flatau, and G. Lévi for helpful discussions on running the DDA code.

References

(1) Schultz, S.; Smith, D. R.; Mock, J. J.; Schultz, D. A. P. *Natl. Acad. Sci. U.S.A.* **2000**, *97*, 996.
(2) Cao, Y. W. C.; Jin, R. C.; Mirkin, C. A. *Science* **2002**, *297*, 1536.
(3) Novotony, L.; Bian, R. X.; Xie, X. S. *Phys. Rev. Lett.* **1997**, *79*, 645.
(4) Calander, N.; Willander, M. *Phys. Rev. Lett.* **2002**, *89*, 143603.
(5) Chaumet, P. C.; Rahmani, A.; Nieto-Vesperinas, M. *Phys. Rev. Lett.* **2002**, *88*, 13601.
(6) Xu, H. X.; Käll, M. *Phys. Rev. Lett.* **2002**, *89*, 24802.
(7) Wenseleers, W.; Stellacci, F.; Meyer-Friedrichsen, T.; Mangel, T.; Bauer, C. A.; Pond, S. J. K.; Marder, S. R.; Perry, J. W. *J. Phys. Chem. B* **2002**, *106*, 6853.
(8) Yin, X.; Fang, N.; Zhang, X.; Martini, I. B.; Schwartz, B. *J. Appl. Phys. Lett.* **2002**, *81*, 3663.
(9) Nie, S.; Emory, S. R. *Science* **1997**, *275*, 1102.
(10) Kneipp, K.; Wang, Y.; Kneipp, H.; Perelman, L. T.; Itzkan, I.; Dasari, R.; Feld, M. S. *Phys. Rev. Lett.* **1997**, *19*, 1667.
(11) Xu, H.; Bjerneld, E. J.; Käll, M.; Börjesson, L. *Phys. Rev. Lett.* **1999**, *83*, 4357.
(12) Barbic, M.; Mock, J. J.; Smith, D. R.; Schultz, S. J. *J. Appl. Phys.* **2002**, *91*, 9341.
(13) Kottman, J. D.; Martin, O. J. F.; Smith, D. R.; Schultz, S. *Chem. Phys. Lett.* **2001**, *341*, 1.
(14) Mock, J. J.; Smith, D. R.; Schultz, S. *Nano. Lett.* **2003**, *3*, 485.
(15) Kottmann, J. P.; Martin Oliver, J. F. *Opt. Lett.* **2001**, *26*, 1096.
(16) Kelly, K. L.; Coronado, E.; Zhao, L. L.; Schatz, G. C. *J. Phys. Chem. B* **2003**, *107*, 668.
(17) Jensen, T.; Kelly, L.; Lazarides, A.; Schatz, G. *Cluster Sci.* **1999**, *10*, 295.
(18) (a) Draine, B. T.; F.;atau, P. J. *J. Opt. Soc. Am. A* **1973**, *11*, 1491. (b) Draine, B. T.; Flatau, P. J. *User Guide for the Discrete Dipole Approximation Code DDSCAT (Version 5a10)*; http://xxx.lanl.gov/abs/astro-ph/0008151v2. (c) Program *DDSCAT.5a*; Draine, B. T., Princeton University Observatory: Princeton, NJ and Flatau, P. J., University of California, San Diego, CA, Scripts Institute of Oceanography, La Jolla, CA.
(19) Félidj, N.; Aubard, J.; Lévi, G. *J. Chem. Phys.* **1999**, *111*, 1195.
(20) Duval Malinsky, M.; Kelly, K. L.; Schatz, G. C.; Van Duyne, R. P. *J. Phys. Chem. B* **2001**, *105*, 2343.
(21) Johnson, P. B.; Christy, R. W. *Phys. Rev. B* **1972**, *6*, 4370.
(22) Tamaru, H.; Kuwata, H.; Miyazaki, H.; Miyano, K. *Appl. Phys. Lett.* **2002**, *80*, 1826.
(23) Moskovits, M. *Rev. Mod. Phys.* **1986**, *57*, 783.
(24) Maier, S. A.; Kik, P. G.; Atwater, H. A. *Appl. Phys. Lett.* **2002**, *81*, 1714.
(25) Quinten, M.; Leitner, A.; Krenn, J. R.; Aussenegg, F. R. *Opt. Lett.* **1998**, *23*, 1331.
(26) Kottmann, J. P.; Martin, O. J. F.; Smith, D. R.; Schultz, S. *J. Microsc. (Oxford)* **2001**, *202*, 60.
(27) Rechberger, W.; Hohenau, A.; Leitner, A.; Krenn, J. R.; Lamprecht, B.; Aussenegg, F. R. *Opt. Commun.* **2003**, *220*, 137.

NL034197F